Title: A stretchable and biodegradable strain and pressure sensor for orthopedic application

Authors: Clementine M. Boutry[1], Yukitoshi Kaizawa[3], Bob C. Schroeder[2], Alex Chortos[1], Anaïs Legrand[3], Zhen Wang[3], James Chang[3], Paige Fox[3*], Zhenan Bao[1*]

Affiliations: [1] Department of Chemical Engineering, Stanford University, Stanford, CA, USA
[2] Department of Chemistry, University College London, 20 Gordon St., London, WC1H 0AJ, UK
[3] Division of Plastic & Reconstructive Surgery, Stanford University Medical Center, Veterans Affairs Palo Alto, Palo Alto, CA, USA

Abstract

The ability to monitor, in real time, the mechanical forces on tendons after surgical repair could allow personalised rehabilitation programs to be developed for recovering patients. However, the development of devices capable of such measurements has been hindered by the strict requirements of biocompatible materials and the need for sensors with satisfactory performance. Here we report an implantable pressure and strain sensor made entirely of biodegradable materials. The sensor is designed to degrade after its useful lifetime, eliminating the need for a second surgery to remove the device. It can measure strain and pressure independently using two vertically isolated sensors capable of discriminating strain as small as 0.4% and the pressure exerted by a grain of salt (12 Pa) without interfering with one another. The device has minimal hysteresis, a response time in the millisecond range, and an excellent cycling stability for strain and pressure sensing, respectively. We have incorporated a biodegradable elastomer which was optimized to improve the strain cycling performances by 54%. An *in vivo* study shows that the sensor exhibits excellent biocompatibility and function in a rat model, illustrating the potential applicability of the device to the real-time monitoring of tendon healing.

Text body

In the U.S. alone, around 14 million people per year suffer from tendon, ligament, and joint injuries[1]. After injury, tissues in the body undergo changes in their native biomechanical properties in order to repairs themselves. This is true for both hard tissues (bones) and soft tissues (tendons, skin, muscles). The objective of surgery and rehabilitation is to restore the tissues to their pre-injury function, with biomechanical properties as close as possible to native properties[2]. A diagnostic tool that measures the biomechanical properties of the repair site in real-time would represent a significant step towards improved assessment of healing and the development of personalized rehabilitation strategies[3].

Current clinical practice for monitoring tissue rehabilitation includes magnetic resonance imaging (MRI) or ultrasound, which provide a snapshot of tissue density and inflammation [4]. Implantable sensors could give continuous information about tissue strain during rehabilitation protocols, as well as during the patient's daily activities, allowing activities to be tailored based on what the tissue can tolerate. Previously described implantable sensors have limited biocompatibility or have been designed for laboratory biomechanics studies rather than clinical practice[4,5].

Implantable sensors for rehabilitation require the measurement of both strain and pressure with high sensitivity and fast response time. The level of strain and strain rate are the most important parameters to characterize the biomechanical properties of soft tissues and their healing stage[5]. The sensor must be able to measure typical tendon strains (<10%) without impeding the natural movement of the tendon[4-6]. Moreover, it should be able to measure the pressure exerted on repaired sites, which directly impacts the healing profile[5,4]. Finally, a sensor entirely made of biodegradable materials would avoid the need for surgical extraction[15,7].

Previously described degradable sensors have either had insufficient sensing performance, or use materials with unproven biocompatibility[8-12]. In addition to biocompatibility, an important feature of our design is the ability of the sensor to discriminate between strain and pressure measurements. Moreover, we designed a new type of flexible strain sensor stacked with a pressure sensor to reduce overall sensor footprint. Our sensor, we believe, satisfies all of the requirements for tissue rehabilitation monitoring, including biodegradability, biocompatibility, and an ability to discriminate strain and pressure stimuli with excellent sensitivity.

After tendon repair, several rehabilitation protocols are used with the objective of finding a balance between active exercise (to prevent tendon adhesions) and immobilization (to protect the integrity of the repair and avoid tendon rupture)[13]. . Early active motion protocols show promising results. However, in current clinical practice, in order to avoid rehabilitation-related injuries, protocols with predefined long time scales and large security margins are applied, resulting in slow and costly rehabilitation protocols, which negatively impacts the quality of life of the patient. The sensor proposed here could be used to assess real-time tissue healing, allowing personalization of a rehabilitation protocol (Fig. 1a)[13,14].

Biodegradable sensor concept and fabrication

Our flexible sensor design incorporates two vertically stacked sensors to allow the independent discrimination of strain and pressure (Fig. 1b). This is a unique aspect of our technology since strain gauges and nanocomposites based strain sensors mounted on a flexible membrane are intrinsically sensitive to both strain and pressure. The strain is determined by measuring the capacitance change between two thin film comb electrodes sliding relative to each other. They are sandwiched between two stretchable elastomer layers. On the other hand, the pressure is measured with a thin, flexible capacitor with our previously reported microstructured elastic dielectric layer for high sensitivity [15,16], while both substrates supporting its top and bottom electrodes, respectively, are bond on only one side with the stretchable package. This design allows the pressure sensor free of influence by the strain.

Our work represents the first time that fully stretchable and biodegradable organic materials are implemented as a biomechanical sensor. We used primarily organic materials because they offer the advantages of versatility in molecular tuning for desirable degradation kinetics, easy process, and mass production capabilities. We selected materials that are well established for their excellent biocompatibility upon degradation, potentially reducing the timeline for clinical translation. In contrast, the cytotoxicity of carbon nanotubes (CNTs) may prevent the use of degradable CNT-PLLA (polylactic acid) composites in biomedical implants[11,12]. Moreover, as illustrated in Fig. 1c and Supplementary Fig. S1, the sensor assembly is a simple benchtop process involving lamination and packaging with a UV-cured sealant. The simple process may be readily scaled.

The key elements of our material design are the two biodegradable elastomers Poly(glycerol sebacate) (PGS)[17] and poly(octamethylene maleate (anhydride) citrate) (POMaC)[18]. Both materials were initially

developed for tissue engineering applications inside the body. PGS is approved by the US Food and Drug Administration (FDA) for biomedical use, while POMaC has been subject to extensive biocompatibility studies, demonstrating its cell and tissue biocompatibility comparable to PLLA control[19,20]. In addition to their established biocompatibility upon degradation, they are excellent candidates for this application in terms of their mechanical properties and the degradation characteristics, which can be tuned by varying the polymerization conditions[17,18]. The electrodes are made of magnesium (Mg) evaporated on top of biodegradable polymer substrate (polylactic acid, PLLA). The biodegradable metal Mg was chosen because

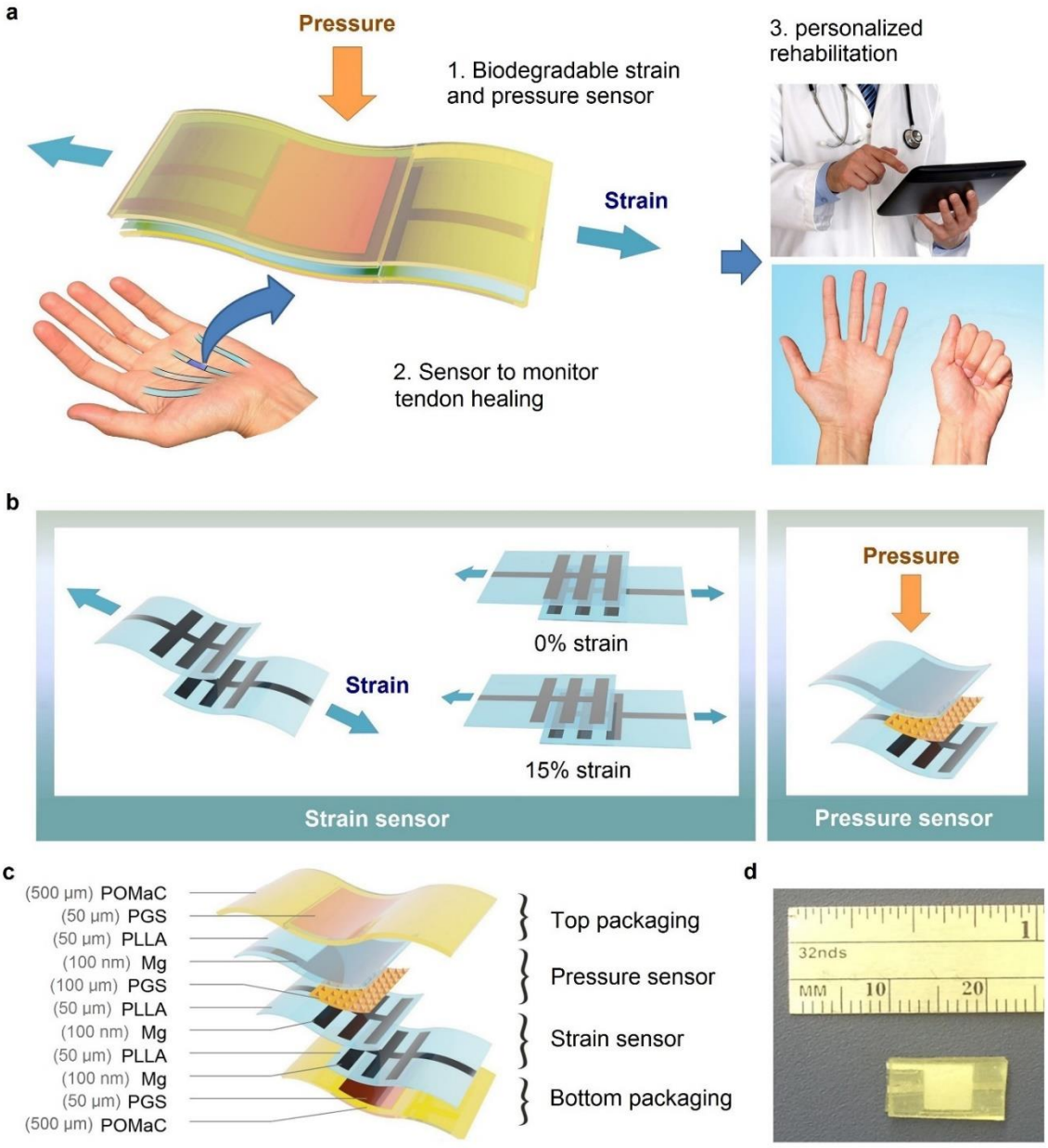

Figure 1: A fully biodegradable and stretchable strain and pressure sensor. a) The sensor can be attached to a tendon for real time healing assessment, allowing the rehabilitation protocol after a tendon repair to be personalized for each patient[13,14]. b) Concepts used for strain and pressure sensing. Strain sensing: Upon applied strain, the two thin film comb electrodes slide relative to each other, resulting in a variation of the capacitance. The range 0-15% for strain sensing is chosen based on the fact that *in vivo* the strain exerted on tendons is lower than 10%[4-6]. Pressure sensing: Upon applied pressure, the variation of the distance

between the top and bottom electrodes results in a variation of the capacitance. The dielectric layer made of a thin, highly compressible, regularly microstructured rubber, enables the sensor to have high pressure sensitivity and fast response time, improving the sensitivity by several orders of magnitude as compared to previously published work based on air gap approach[15,8]. c) Materials and overall assembly of the fully biodegradable strain and pressure sensor. The biodegradable elastomer PGS (Poly(glycerol sebacate))[17], is used as a dielectric layer for the capacitor constituting the pressure sensor[15]. It is also used in the strain sensor architecture as a stretchable non-sticking layer allowing the electrodes to slide relative to each other. The biodegradable elastomer POMaC (poly(octamethylene maleate (anhydride) citrate)), is used for the strain sensor and packaging[18]. POMaC is a soft stretchable biodegradable elastomeric biomaterial synthesized from citric acid, maleic anhydride, and 1,8-octanediol, which is able to mimic the mechanical properties of a wide range of soft biological tissues[18]. d) Picture of the assembled sensor.

of its easy processing, biocompatibility, and rapid rates of hydrolysis. It has been in use for more than a decade in clinical trials in applications such as biodegradable stents[21], and it is considered as an essential nutrient with a daily allowance of 0.7g[22]. Upon degradation of the sensor, body fluids will eventually penetrate through the packaging layer, resulting in the corrosion of Mg with the formation of highly soluble magnesium oxides that will be evacuated via natural tracks[23].

POMaC elastomer biodegradation and resistance to cycling

The desired material properties for the POMaC elastomer are defined based on two key sensor requirements: 1) The sensor must be stretchable with a low tensile modulus in order to avoid limiting motion or hindering the healing process. 2) The sensor must be resistant to cycling without breaking (to support repeated rehabilitation exercises), when exposed to physiological conditions[5].

The target initial tensile modulus for POMaC is defined to be ~0.5 MPa, soft enough for high mechanical compliance and stiff enough for easy sensor assembly and manipulation. As a reference, the tensile modulus of human hand flexor tendons is 200-300 MPa[24]. As illustrated in Fig. 2a, after synthesis of pre-POMaC, the POMaC elastomer can be further polymerized following different paths, resulting either in PPOMaC (UV irradiation polymerization), EPPOMaC (UV irradiation followed by oven post polymerization), or EPOMaC (oven post polymerization)[18]. Different mechanical properties and biodegradation profiles are expected for PPOMaC, EPPOMaC and EPOMaC when exposed to physiological media, since the crosslinking mechanisms and chemical bonds involved are different[18].

An *in vitro* degradation study was performed over 8 weeks, with samples incubated in phosphate buffered saline (PBS) solution at 37°C. The fatigue life (number of cycles before rupture) was tested using the scheme in Fig. 2b, and the tensile moduli upon degradation are shown in Fig. 2c-d. This study shows the superiority of EPPOMaC compared to other polymerization conditions, with 54% longer fatigue life. The slower degradation rate of the tensile modulus in EPPOMaC as compared to EPOMaC (11% and 14% per week, respectively) is explained by additional non-hydrolysable UV-induced crosslinks retaining the mechanical cohesion longer in EPPOMaC.

Biodegradable strain and pressure sensor characterization

The sensor performance is illustrated in Fig. 3. Fig. 3a shows the strain sensor response curves from five consecutive linear loading-unloading cycles. After applying a constant strain of 10% and releasing to 5% for more than 20 000 cycles, C_{min} and C_{max} increase by 11% and 8%, respectively (Fig. 3g). Moreover, there is a one order of magnitude increase in sensitivity to strain as compared to previously reports for transient strain sensors[10]. Indeed, for an applied strain of 15%, the relative capacitance change of our sensor is $\Delta C/C_0$ = ~50%, where C and C_0 are the capacitances with and without applied strain and $\Delta C = |C - C_0|$. As

a comparison, degradable Si-based strain gauges exhibited a signal change of ~5% for the same applied strain[10].

Figure 3b shows the pressure sensor response curves from six consecutive cycles for sensors with POMaC packaging for encapsulation. After applying a constant pressure of 45 kPa and releasing to 15 kPa for more than 30 000 cycles, C_{min} increased only by 5% and C_{max} decreased by only 2%. Moreover, the pressure sensitivity is 0.7 ± 0.4 kPa^{-1} in low pressure regime (p < 1 kPa) and 0.13 ± 0.03 kPa^{-1} at higher pressures (5 < p < 10 kPa). These values are in good agreement with our previous results[15]. These pressure sensitivities are one to three orders of magnitude higher than previously published degradable sensors[8]. Consecutive pressure measurements with increasing maximum pressures (Supplementary Fig. S2) indicate that the

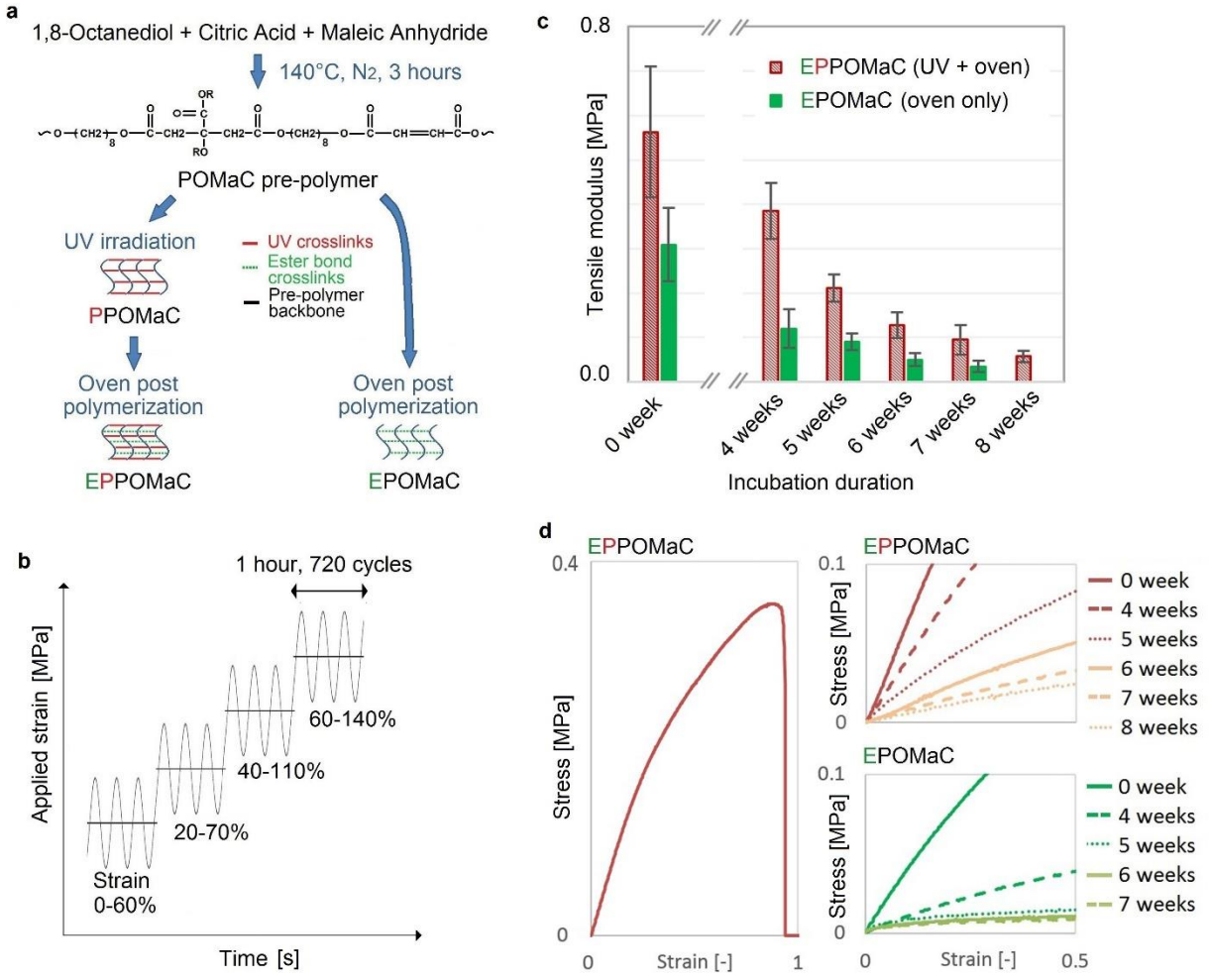

Figure 2: Investigations of the POMaC elastomer used in the strain sensor and as packaging material to improve resistance to cycling upon biodegradation. a) POMaC polymerization paths. In EPOMaC, the crosslinking is a polycondensation without photocrosslinking, resulting in ester bond crosslinked POMaC. In PPOMaC, the exposure to UV irradiation results in a photocrosslinking with free radical polymerization through the vinyl carrying carbons. In EPPOMaC, post-polymerization results in further crosslinking the polymer through the available free functional groups of citric acid to yield ester bond crosslinked photocrosslinked POMaC[18]. b) Schematic of the strain cycles applied on the POMaC samples to test their fatigue life (number of cycles before rupture). The applied cycling strain is initially 0 to 60% and increases every hours (720 cycles) resulting eventually in samples rupture. PPOMaC produced with 48 hours UV exposure results in samples with the target tensile modulus of 0.5 MPa. However, because of the sample's sticky gel aspect making the manipulation challenging, PPOMaC is not further considered for sensor application. EPPOMaC produced with 20 minutes UV exposure followed by 48 hours oven post polymerization also results in a tensile modulus of 0.5 MPa. EPPOMaC exhibits a 33% increase in fatigue life compared to PPOMaC. EPPOMaC produced with

48 hours oven post polymerization results in samples with a tensile modulus of 0.3 MPa, below the 0.5 MPa target value. The fatigue life is found to be ~3 times higher in EPOMaC as compared to EPPOMaC. This is explained by the lower tensile modulus of EPOMaC, resulting in a more elastic, less brittle material. c) POMaC elastomer *in vitro* degradation study. When POMaC is exposed to physiological media, the tensile modulus decreases with a rate of -11% per week for EPPOMaC and 14% per week for EPOMaC. The difference in degradation rates is explained by additional non-hydrolysable UV links that maintain the mechanical cohesion in EPPOMaC as compared to EPOMaC. Cycling tests are performed on EPPOMaC and EPOMaC after *in vitro* degradation, showing the superiority EPPOMaC as compared EPOMaC, with 54% higher fatigue life. This result is found for materials with identical tensile moduli (EPPOMaC incubated 6 weeks and EPOMaC incubated 4 weeks, having both a tensile modulus of 0.14 MPa). This condition allows for comparison of the cycling performances. d) Stress-strain characteristics for EPOMaC and EPPOMaC for various incubation durations.

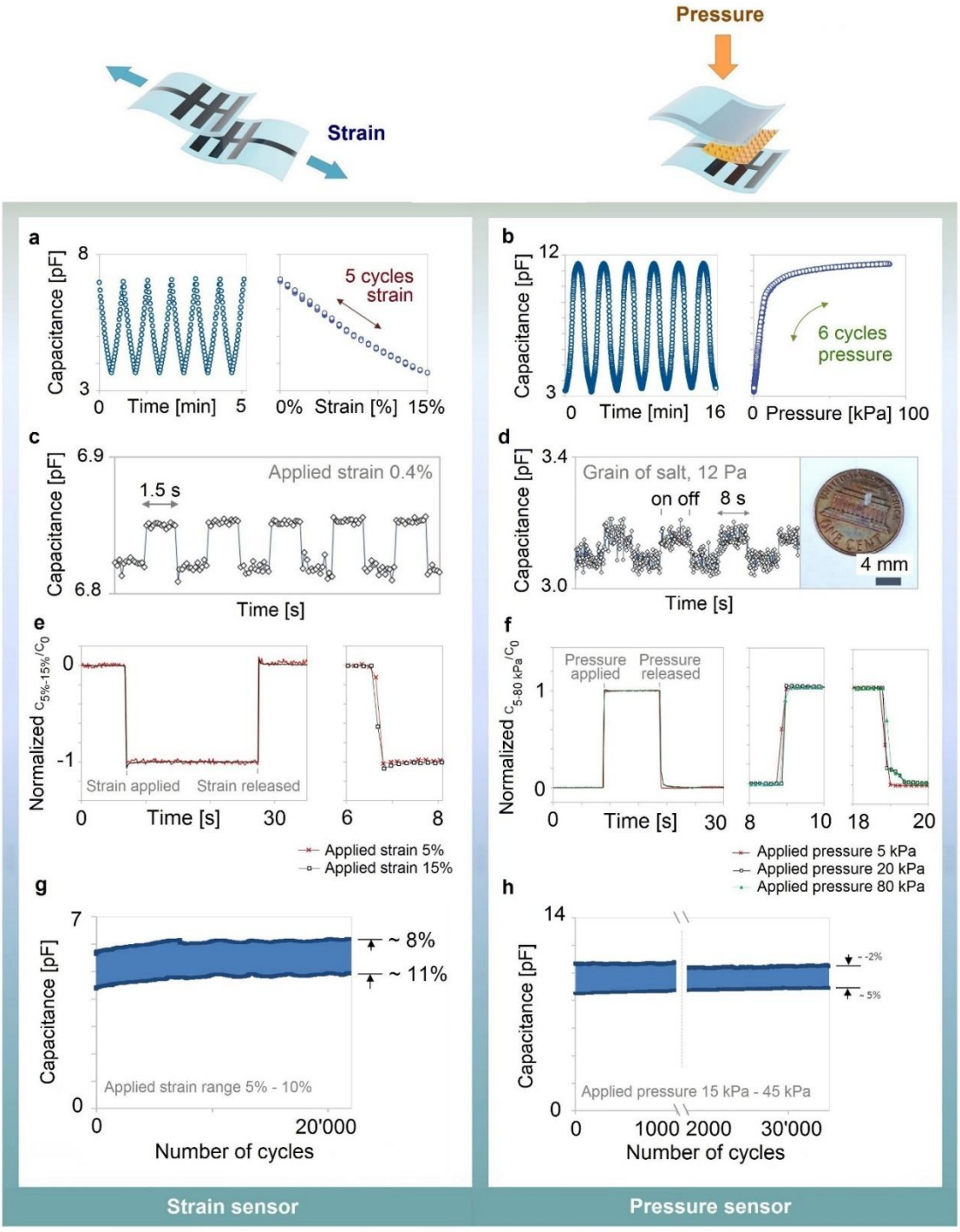

Figure 3: Response characteristics of the biodegradable strain and pressure sensor. a) Strain response curve from five consecutive linear loading-unloading cycles (applied strain 0-15%). The hysteresis is observed to be negligible. b) Pressure response curve from six consecutive cycles (applied pressure 0-100 kPa). Again negligible hysteresis is observed. Evaluation of c) the smallest detectable strain (signal-to-noise ratio *SNR* = ~2.1, no averaging applied, real time measurement) and d) the smallest detectable pressure (the signal corresponds to the *SNR* detection limit, again with no averaging applied, real time measurement). Sensor response time e) to applied strain and f) to applied pressure. Cycling tests and stability of g) the strain response (applied strain 5% to 10%) and h) the pressure response (applied pressure 15 kPa to 45 kPa).

device output is highly reproducible even with large applied pressures up to 430 kPa. The high sensitivity for small applied strains and pressures is illustrated in Fig. 3c and 3d, respectively, where strains as low as 0.4% and pressures as low as 12 Pa (corresponding to a grain of salt) are successfully measured. In addition, the sensor can measure strain and pressure independently from each other as illustrated in Supplementary Fig. S3. Our device's fast response time in the millisecond range is illustrated in Fig. 3e and 3f for strain and pressure sensing, respectively. Moreover, the strain and pressure response curves of the sensor can be reproducibly cycled thousands of times. The fast response time and cycling durability satisfy the requirements for real-time bio-monitoring for orthopedic rehabilitation.

Sensor *in vivo* function and biocompatibility

In vitro and *in vivo* studies were performed to verify that the biodegradable strain and pressure sensor will be functional (Fig. 4) and well tolerated inside the body (Fig. 5). The sensor, designed to stay operational *in vivo* for more than 2 weeks, slowly degrades after its period of use when immersed in physiological media (Supplementary Fig. S4). This period corresponds to the duration of interest to monitor tendon healing, with rehabilitation protocols starting as early as 24h postoperatively[13,14]. The performance of the sensor immersed in PBS solution at 25°C is assessed over 5 weeks and compared to a reference sensor made of non-biodegradable materials (Supplementary Fig. S5). Stable operation over 2 to 3 weeks is observed, with sensitivity comparable to the reference sensor, until the degradation of the Mg electrodes occurs (Supplementary Fig. S5b-e). As shown in Fig. 4a, the sensor can be successfully used to measure physiological strain signal on a real tendon.

Sensors were implanted subcutaneously on the back of Sprague Dawley rats (Fig. 4b). Strain and pressure stimuli were applied *in vivo* as illustrated in Fig. 4c. The corresponding signals are successfully recorded after 3.5 weeks of implantation as shown in Fig. 4d and 4e for pressure and strain sensing, respectively. The high sensitivity of our device both in strain and pressure assessment is illustrated in these figures where a zoom on the baseline signal shows the recording of the respiration of the animal. The degradation behavior of both POMaC and PGS is based on surface erosion rather than bulk erosion[25,18,20]. This mechanism allows the POMaC packaging to provide an efficient protection against penetration of body fluids inside the sensor, preventing the premature degradation of the Mg electrodes.

Moreover, the animals tolerated the presence of the sensor with no long-term adverse inflammatory reaction as quantitatively assessed in Fig. 5. Both immunohistochemistry and Hematoxylin and eosin staining show the good biocompatibility of POMaC after 8 weeks of implantation, with no statistically significant difference between POMaC and silicone (control) sample.

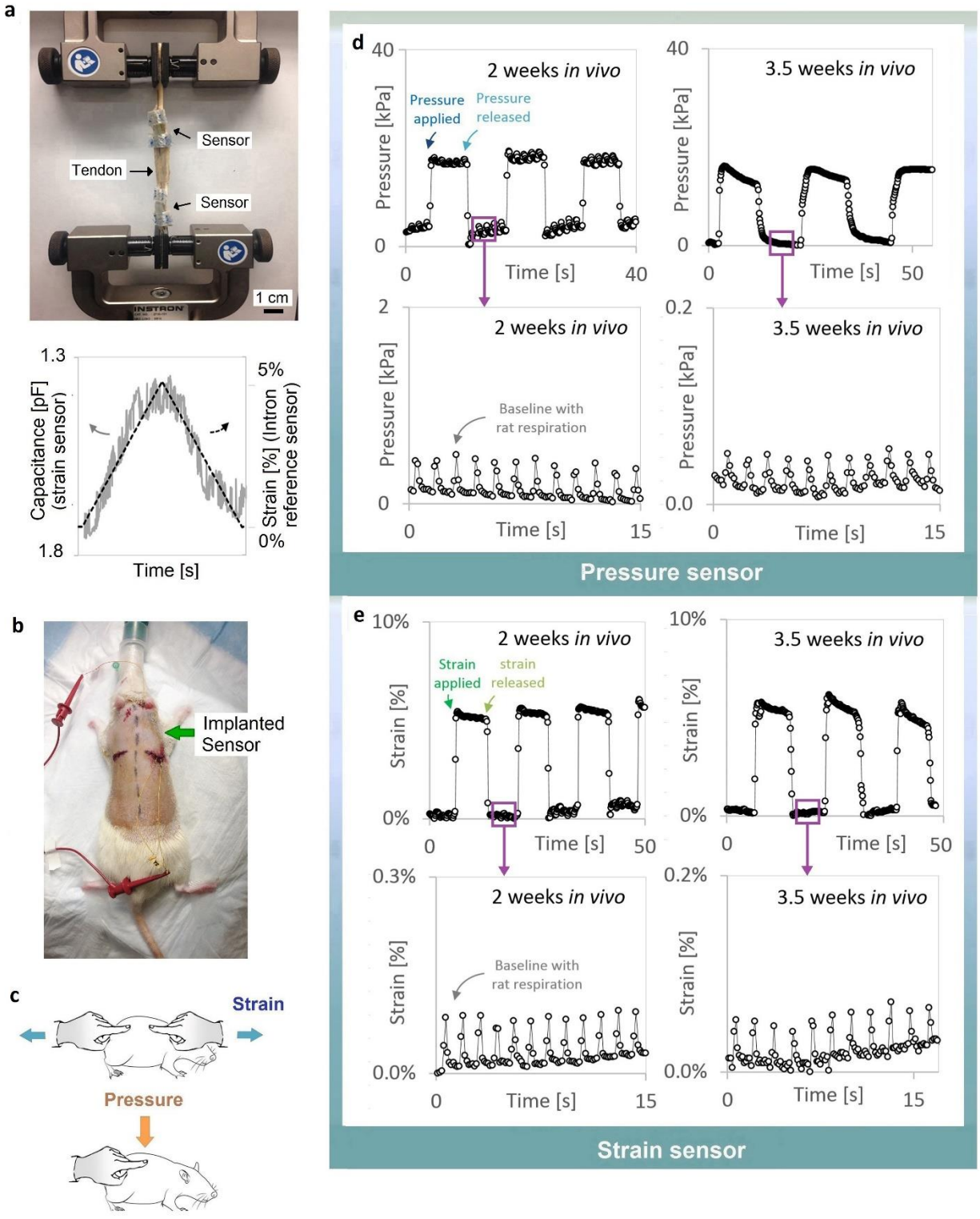

Figure 4: *In vitro* and *in vivo* study of the biodegradable strain and pressure sensor. a) Top: Sensor fixed on a tendon mounted in a stress-strain Instron microtester, allowing for the measurement of the tensile modulus of the tendon, 201 MPa, which is in good agreement with literature (0 to 14% strain, strain rate 0.25mm/s)[24]. Bottom: The signal measured with the strain sensor is compared to the reference microtester signal, showing a linear relation, with deviation from linear fit better than R^2 = 89% (R^2 = coefficient of determination). *In vivo* study: b) The biodegradable strain and pressure sensor was subcutaneously implanted on

the back of a Sprague Dawley rat. c) Strain and pressure signals applied on the implanted sensor *in vivo*. d) Pressure signal recorded after 2 weeks (top left) and 3.5 weeks (top right) after sensor implantation. Corresponding baseline showing the respiration of the animal recorded with the pressure sensor, after 2 weeks (bottom left) and 3.5 weeks (bottom right) *in vivo*. e) Strain signal recorded after 2 weeks (top left) and 3.5 weeks (top right) after sensor implantation. Corresponding baseline showing the respiration of the animal recorded with the strain sensor, after 2 weeks (bottom left) and 3.5 weeks (bottom right) of sensor implantation.

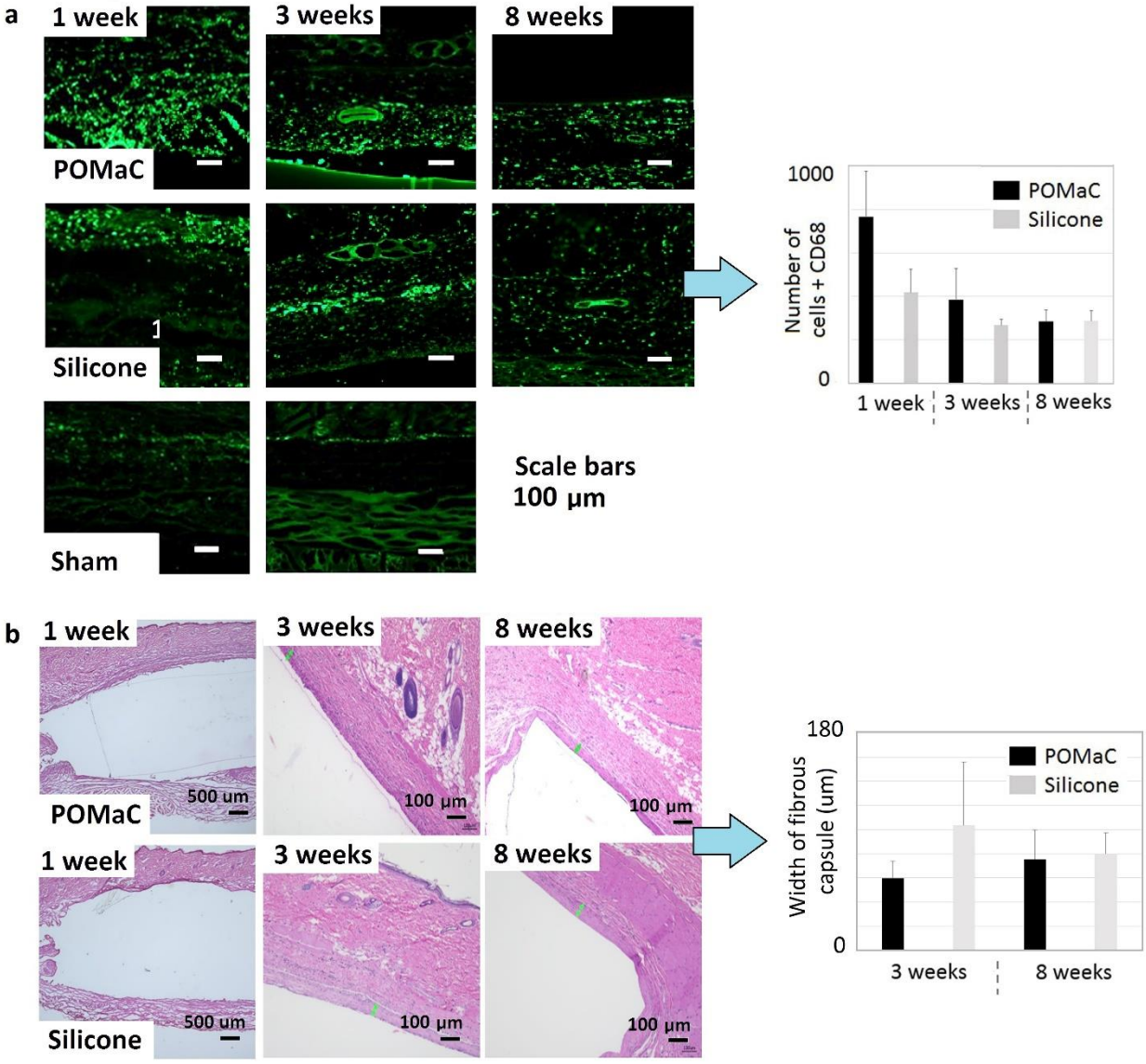

Figure 5: The biocompatibility of POMaC and silicone (control) are evaluated *in vivo*. a) Results of immunohistochemistry (IHC). After one week, the number of the CD68 positive cells - indicating an inflammatory reaction - is larger in the tissues surrounding POMaC sample than in the tissues surrounding silicone sample. However, after 3 weeks and 8 weeks of implantation, there is no statistically significant difference between POMaC and silicone (control) sample, indicating good biocompatibility of POMaC *in vivo*. b) Results of paraffin sections for hematoxylin and eosin (H&E) staining. A fibrous capsule of comparable width is formed around both the POMaC and silicone (control) samples at 1, 3 and 8 weeks.

Conclusions

The high sensitivity, fast time response, and biodegradability of our sensor means that it could also be of value in biomedical applications beyond orthopedic rehabilitation monitoring. For example, it could be relevant to cardiovascular patches[26] and reconstructive surgery[27], where the monitoring of mechanical deformations and pressures real time *in vivo* will allow for refined and personalized medicine. Future research will consist of developing a wireless system made entirely of biodegradable materials, including the circuit used for wireless transmission of measured signals though the skin.

Methods

Sensor Fabrication

Synthesis of POMaC top and bottom encapsulation layer - The synthesis of PPOMaC and EPPOMaC is performed as described in reference [18]. Briefly, maleic anhydride (Fluka, CAS 108-31-6), citric acid (Sigma Aldrich, CAS 77-92-9) and 1,8-octanediol (Sigma-Aldrich, CAS 629-41-4) are mixed in a 3 necked round-bottom flask with a molar feed ratio of 3:2:5, respectively. The flask content is heated at an initial temperature of 160°C and stirred under nitrogen atmosphere. After the mixture melts, the temperature is set to 140°C and it is continuously stirred under nitrogen for 3 hours. In order to remove any of the unreacted monomers and oligomers, the pre-polymer is dissolved in tetrahydrofuran (THF, about 5 g in 20 ml), and purified by drop wise precipitation into 2 liters of deionized water. Photocrosslinked POMaC networks (PPOMaC) are formed by crosslinking through free radical polymerization. The photoinitiator 2-Hydroxy-4'-(2-hydroxyethoxy)-2-methylpropiophenone (CAS 106797-53-9, 0.06 g) is dissolved in ethyl acetate (1 ml) and mixed with pre-POMaC (6 g) using a speed mixer at 3000 rpm for 3 minutes. The solution is then poured into a PTFE container. After solvent evaporation, the sample is first exposed to a 365 nm ultraviolet light lamp (25W) for 20 minutes. It is then cured in oven at 80°C for 48 hours to complete the polymerization process to give EPPOMaC, which is used as the encapsulation layer (thickness 0.8 mm).

Preparation of the POMaC elastomers - In this study, three different POMaC networks are investigated, with polymerization protocols similar as described before[18]. Photocrosslinked POMaC (PPOMaC) is produced by exposure to UV irradiation, where the free radical polymerization is initiated to crosslink pre-POMaC through vinyl carrying carbons (48 hours UV exposure). Ester bond crosslinked POMaC (EPOMaC) is produced through polycondensation without photocrosslinking (48 hours oven post polymerization at 80 degree Celcius). Finally, ester bond crosslinked photocrosslinked POMaC (EPPOMaC) is produced by further crosslinking PPOMaC through the available free functional groups of citric acid (20 minutes UV exposure followed by 48 hours oven post polymerization at 80 degree Celcius). The cycling tests in Fig. 2b are performed at a speed of ~5 cycles/min.

Synthesis of PGS and fabrication of microstructured dielectric layer for pressure sensor– PGS is synthesized based on previously published methods[17,15], where an equimolar mixture of glycerol and sebacic acid is reacted at 120 degree Celcius under nitrogen for 24 h, resulting in a viscous uncrosslinked PGS pre-polymer. The fabrication of the PGS microstructured dielectric layer is similar as our previous report[15]. Briefly, the PGS pre-polymer is further polymerized in oven at 130 degree Celcius in vacuum for 24 hours. Afterwards the highly viscous pre-polymer is cured between the PDMS mold and a bare silicon wafer, both treated with a non-adhesive layer evaporated in vacuum ((tridecafluoro-1,1,2,2-tetrahydrooctyl)trichlorosilane, Gelest, USA, CAS 78560-45-9). Two-dimensional arrays of square pyramids are formed into PGS from the PDMS mold. The PDMS mold itself is fabricated from a (100) Si-wafer mold having etched arrays of pyramidal recesses. After being cured at 130 degree Celcius in vacuum

for 15 hours, the ~150 µm-thick PGS film is peeled off and laminated with the bottom and top electrodes. In addition to the PGS layer used as a dielectric into the pressure sensor, two additional PGS layers are used as non-sticking layers, allowing the strain sensor top and bottom electrodes to slide relative to each other. These two PGS layers are fabricated as described above, except that the PDMS mold has no square pyramids.

Fabrication of biodegradable metal electrodes – The electrodes are fabricated by evaporating magnesium (100 µm-thick electrode) on top of a 50 µm-thick polylactide layer (PLLA, Goodfellow) after having exposed the substrate surface to oxygen plasma. The electrodes are operated below the standard potential of -1.23 V (corresponding to the electrolysis of water) to avoid any unwanted redox reaction at the interface of Mg electrodes with body fluids and stay within the safe water window[28].

Sensor Assembly – The sensor is assembled as described in Supplementary Fig. S1. The layers are laminated on top of each other and the packaging is closed using a layer of UV-cured pre-POMaC as sealing agent.

Characterization of the sensor

Strain and pressure response measurement setup: The pressure measurement setup consists in a motorized vertical stage used in combination with a force gauge (digital force gauge series 5, Mark-10, USA), while the capacitance of the sensor is measured with an E4980A Agilent Precision LCR meter. The strain measurement setup consists in a motorized horizontal stage, the capacitance of the sensor being measured with the LCR meter. Measurements are performed in controlled temperature and humidity atmosphere at 23 ± 1 °C and 50 ± 10% relative humidity.

In vivo sensor function assessment

Implantation of the sensor **-** Three Sprague Dawley (SD) rats (12w, 300-350g, male, ENVIGO) were cared for in compliance with regulations of animal care and use committee of Veteran Affair Palo Alto Health Care System Research Administration. Sensors were implanted in a subcutaneous paravertebral pocket under isoflurane inhalation anesthesia. Each animal was administered a dose enrofloxacin (Bayer Corp., Leverkusen, Germany) for antibiotic prophylaxis preoperatively and buprenorphine (Reckitt Benckiser Pharmaceuticals, Inc., Richmond, VA) for pain control post-operatively. The rats were monitored throughout the study. Wire and surgical sites were covered with an occlusive dressing between tests.
Sensor Function - The function of the sensor was tested on days 0, 1, 3, 5, 7, 10, 14, 17, 21, and 24 after implantation. Tests were performed under isoflurane inhalation anesthesia.

In vivo Biocompatibility Assessment

Implantation and harvest of materials - The biocompatibility of POMaC and silicone (control) were evaluated histologically. Nine SD (12-14w, 300-350g, male, ENVIGO) rats were used for 1, 3, and 8 weeks evaluations. Three rats for each time point evaluation underwent sham operations or material implantation surgeries. Under isoflurane inhalation anesthesia, subcutaneous paravertebral pockets were created on right and left sides of the upper backs of the rats. Six pockets of the three rats were randomly divided into the group of POMaC, silicone, and sham. In the POMaC and silicone group, the tested materials were put into the pockets after sterilization. In the sham group, the wound was closed without implantation of a materials. The rats were monitored throughout the study. At 1, 3, and 8 weeks after implantation, rats were euthanized by CO2 inhalation, and the materials and their surrounding tissues were harvested. After harvest, the samples were cut in a half longitudinally; half for paraffin sections for hematoxylin and eosin (H&E) staining and the other half for frozen sections for immunohistochemistry (IHC).

H&E Analysis - After fixation of the samples in 10% formalin, four 5-µm-thick paraffin sections were prepared per material at each time point, followed by H&E staining. The width of fibrous capsules was measured at three points per section, which were selected at random on the superficial side of the capsule. The mean value of the three measurements was calculated and used for evaluations.
Immunohistochemistry for CD68 - After fixation of the sample in 4% paraformaldehyde (PFA), four 10-µm-thick longitudinal frozen sections were prepared per material at each time point for IHC for CD68. After antigen retrieval using proteinase K (PK; Sigma-Aldrich, St Louis, MO, USA), donkey serum (Sigma-Aldrich) was added to the slides as a blocking procedure. The slides were incubated with primary antibodies [rabbit polyclonal anti-CD68 antibodies (1:100; Abcam, Cambridge, UK)], followed by incubation with secondary antibodies [donkey anti-rabbit IgG (H+L) whole antibodies (1:200; CFTM488 fluorescent reagents; Biotium, Fremont, CA, USA)]. The slides were viewed under fluorescence microscope (KEYENCE BZ-X700; KEYENCE Osaka, Japan). More than six fields at 10x magnification per section were selected at random in the area within 1-mm from the material on the superficial side. The number of the CD68 positive cells in the fields was measured using image J analysis software and the mean value was calculated per section.
Statistical analysis - All data are expressed as the mean ±standard deviation (SD). The data were compared using an unpaired t test. P values < 0.05 were considered statistically significant.

The data that support the plots within this paper and other findings of this study are available from the corresponding author upon reasonable request.

References

1. Yang, G., Rothrauff, B.B. & Tuan, R.S. Tendon and Ligament Regeneration and Repair: Clinical Relevance and Developmental Paradigm. *Birth Defects Res C Embryo Today* **99**, 203–222 (2013).
2. Place E.S., Evans, N.D. & Stevens M. M. Complexity in biomaterials for tissue engineering. *Nature Mater.* **8**, 457–470 (2009).
3. McGilvray, K.C. *et al.* Implantable microelectromechanical sensors for diagnostic monitoring and post-surgical prediction of bone fracture healing. *J. Orthop. Res.* **33**, 1439–1446 (2015).
4. Bogaerts, S., Desmet, H., Slagmolen, P. & Peers, K. Strain mapping in the Achilles tendon - A systematic review. *J. Biomech.* **49**, 1411–1419 (2016).
5. Roriz, P. *et al.* From conventional sensors to fibre optic sensors for strain and force measurements in biomechanics applications: A review. *J. Biomech.* **47**, 1251–1261 (2014).
6. Kubo, K., Kanehisa, H., Kawakami, Y. & Fukunaga, T. Influence of static stretching on viscoelastic properties of human tendon structure *in vivo*. *J. Appl. Physiol*. **90**, 520-527 (2001).
7. Waugh, C.M., Blazevich, A.J., Fath, F. & Korff, T. Age-related changes in mechanical properties of the Achilles tendon. *J. Anat. 220*, 144–155 (2012).
8. Luo, M., Martinez, A.W., Song, C., Herrault, F. & Allen, M.G. A Microfabricated wireless RF pressure sensor made completely of biodegradable materials. *J. Microelectromech. Syst*. **23**, 4–13 (2014).
9. Hwang, S.W. *et al.* A physically transient form of silicon electronics. *Science* **28**, 1640–1644 (2012).
10. Xu, L. *et al.* 3D multifunctional integumentary membranes for spatiotemporal cardiac measurements and stimulation across the entire epicardium. *Nat. Commun.* **25**, 1–10 (2014).
11. Liu, Y., Chakrabartty, S., Stamatis Gkinosatis, D., Mohanty, A. K. & Lajnef, N. Multi-walled carbon nanotubes/Poly(L-lactide) nanocomposite strain sensor for biomechanical implants*. Biomedical Circuits and Systems Conference BIOCAS 2007* 119–122 (2007).
12. Singh, S. & Singh Nalwa, H. Nanotechnology and health safety - Toxicity and risk assessments of nanostructured materials on human health. *J. Nanosci. Nanotechnol.* **7**, 3048–3070 (2007).
13. Hein, C., Wilton, P. & Wongworawat M. D. Review of Flexor Tendon Rehabilitation Protocols Following Zone II Repair. *Crit. Rev. Phys. Rehabil. Med.* **27**, 11–18 (2015).
14. Saini, N., Kundnani, V., Patni, P. & Gupta, S.P. Outcome of early active mobilization after flexor tendons repair in zones II–V in hand. *Indian J. Orthop*. **44**, 314–321 (2010).
15. Boutry, C.M., Nguyen, A., Omotayo Lawal, Q., Chortos, A., Rondeau-Gagné, S. & Bao, Z. A Sensitive and Biodegradable Pressure Sensor Array for Cardiovascular Monitoring. *Adv. Mater*. **27**, 6954–6961 (2015).
16. Mannsfeld, S.C.B., Tee, B.C.K., Stoltenberg, R., Chen, C.V.H.H., Barmann, S., Muir, B.V.O., Sokolov, A.N., Reese, C. & Bao, Z. Highly sensitive flexible pressure sensors with microstructured rubber dielectric layers. *Nat. Mat.* **9**, 859-864 (2010).
17. Wang, Y., Ameer, G.A., Sheppard, B.J. & Langer, R.A tough biodegradable elastomer. *Nat. Biotechnol*. **20**, 602–606 (2002).
18. Tran, R.T., Thevenot, P., Gyawali, D., Chiao, J.C., Tang, L. & Yang, J. Synthesis and characterization of a biodegradable elastomer featuring a dual crosslinking mechanism. *Soft Matter* **6**, 2449–2461 (2010).
19. Zhang, B. *et al*. Biodegradable scaffold with built-in vasculature for organ-on-a-chip engineering and direct surgical anastomosis. *Nature Mater.* **15**, 669–678 (2016).
20. Davenport Huyer, L. *et al.* Highly Elastic and Moldable Polyester Biomaterial for Cardiac Tissue Engineering Applications. *ACS Biomater. Sci. Eng.* **2**, 780–788 (2016).
21. Purnama, A., Hermawan, H. & Mantovani, D. Biodegradable metal stents: A focused review on materials and clinical studies. *J. Biomater. Tissue Eng.* **7**, 868–874 (2014).
22. Zheng, Y.F., Gu, X.N. & Witte, F. Biodegradable metals. *Mater. Sci. Eng. R*. **77**, 1–34 (2014).

23. Yin, L., Cheng, H., Mao, S., Haasch, R., Liu, Y., Xie, X., Hwang, S.-W., Jain, H., Kang, S.-K., Su, Y., Li, R., Huang, Y., Rogers, J.A. Dissolvable metals for transient electronics. Adv. Funct. Mater. 24, 645–658 (2014).
24. Huang, H., Zhang, J., Sun, K., Zhang, X. & Tian, S. Effects of repetitive multiple freeze–thaw cycles on the biomechanical properties of human flexor digitorum superficialis and flexor pollicis longus tendons. *Clin. Biomech.* **26**, 419–423 (2011).
25. Rai, R., Tallawi, M., Grigore, A., Boccaccini, A.R. Prog. Polym. Sci. Synthesis, properties and biomedical applications of poly(glycerol sebacate) (PGS): A review. 37, 1051–1078 (2012).
26. Kapnisi, M., Mawad, D., Rathnayake-Arachchige, D., Conway, P. & Stevens, M. Auxetic Micropatterning of a Cell Adhesive-Conductive Composite for Cardiac Tissue Engineering. *Proc. San Francisco MRS* (2015).
27. Bannister, M. & Ah-See, K.W. Enhanced recovery programmes in head and neck surgery: systematic review. *J. Laryngol. Otol*. **129**, 416–420 (2015).
28. Pour Aryan N., Kaim H., Rothermel A. Stimulation and recording electrodes for neural prostheses. Springer (2015).

Acknowledgements

C.M.B. acknowledges postdoctoral fellowship support by the Swiss National Science Foundation (postdoc mobility fellowship number P2EZP2_152118) and the European Commission (Marie-Curie international outgoing fellowship grant number 622362). Part of this work was performed at the Stanford Nano Shared Facilities (SNSF). B.C.S. acknowledges the National Research Fund of Luxembourg for financial support (Project 6932623).

Author Contributions

C.M.B. is the main contributor to this work, elaborating the sensor concept, developing new fabrication processes, performing all experiments for materials investigations, devices characterization, data collection for *in vitro* and *in vivo* experiments, data analysis and interpretation, and drafting of the article. B.C.S. contributed to the POMaC investigation including polymer synthesis, chemical properties characterization, data analysis and interpretation, and provided critical revision of the article. A.C. contributed to the drafting of the article and provided critical revision. Y.K. performed all surgeries related to the *in vivo* studies, including design of the *in vivo* studies, development of the protocols, sensors implantation and operation studies, and materials biocompatibility studies. He also worked on data analysis and interpretation, and provided contribution to the drafting and critical revision of the article. A.L. performed all surgeries related to the tendon *in vitro* studies, and worked on data analysis and interpretation. Z.W., J.C. and P.F. contributed to the design of the *in vivo* studies, working on the protocols and data interpretation. P.F. also provided contribution to the drafting and critical revision of the article. Z.B. provided contribution to the development of sensor concept, fabrication processes and materials investigations, devices characterization, data interpretation, and critical revision of the article.

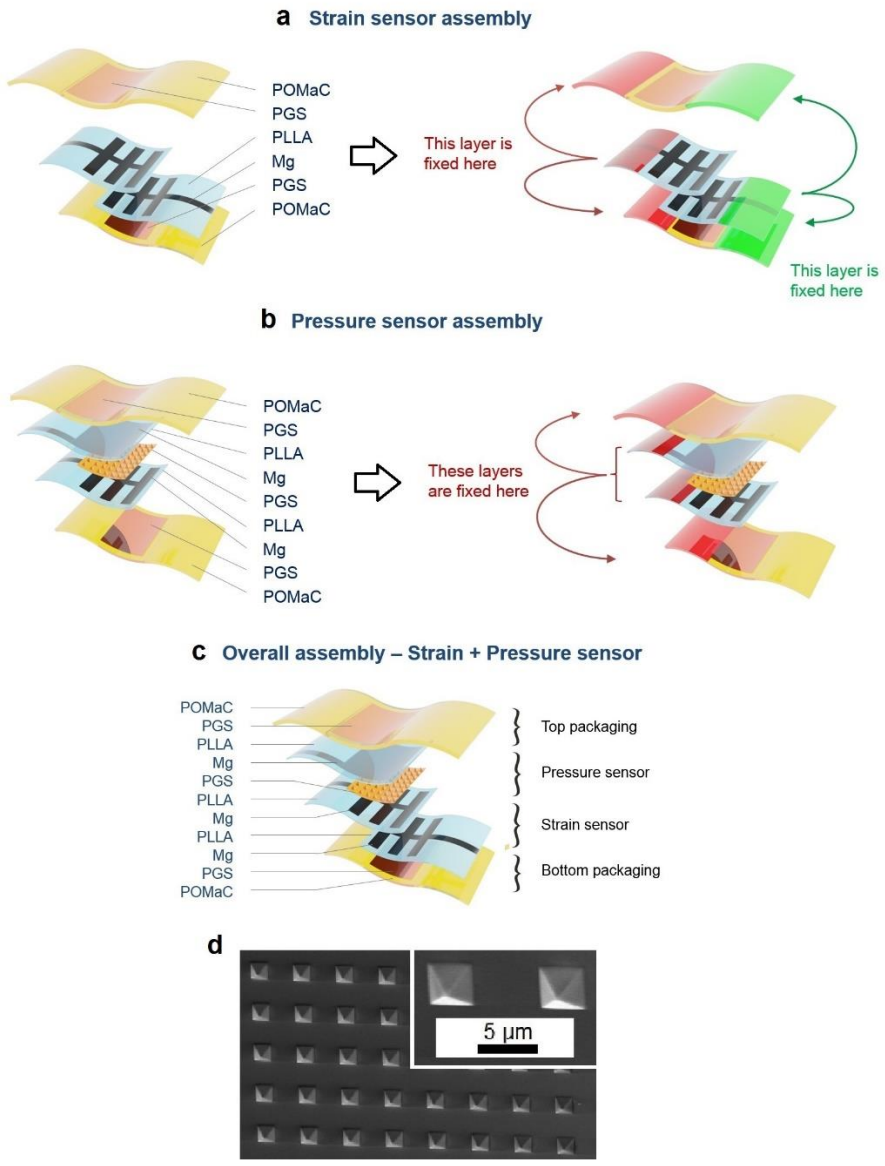

Supplementary Figure S1: a) Strain sensor assembly, b) pressure sensor assembly, and c) overall assembly of the biodegradable strain and pressure sensor. d) SEM images of the microstructured PGS film used as a dielectric layer into the pressure sensor. Two-dimensional arrays of square pyramids are formed into PGS from a PDMS mold (adapted from reference [15]).

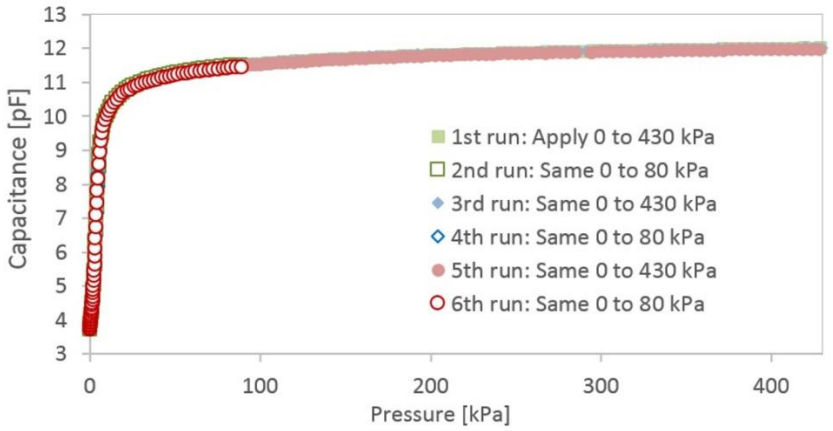

Supplementary Figure S2: Device response at applied pressures in the range 0 to 430 kPa. The robustness of the sensor is illustrated by the unaltered pressure response curves after several runs. 1st run: a pressure is applied from 0 to 430 kPa and back, twice. 2nd run: the same is performed for a pressure ranging from 0 to 80 kPa. A total of 6 runs are performed, with reproducible pressure response curves that illustrate the sensor robustness at high pressures. The maximum pressure that is experimentally applied on the sensors is 430 kPa, corresponding approximately to a weight of 4.4 kg applied on an area of 1 cm^2 (this maximum pressure corresponds to experimental setup limitation).

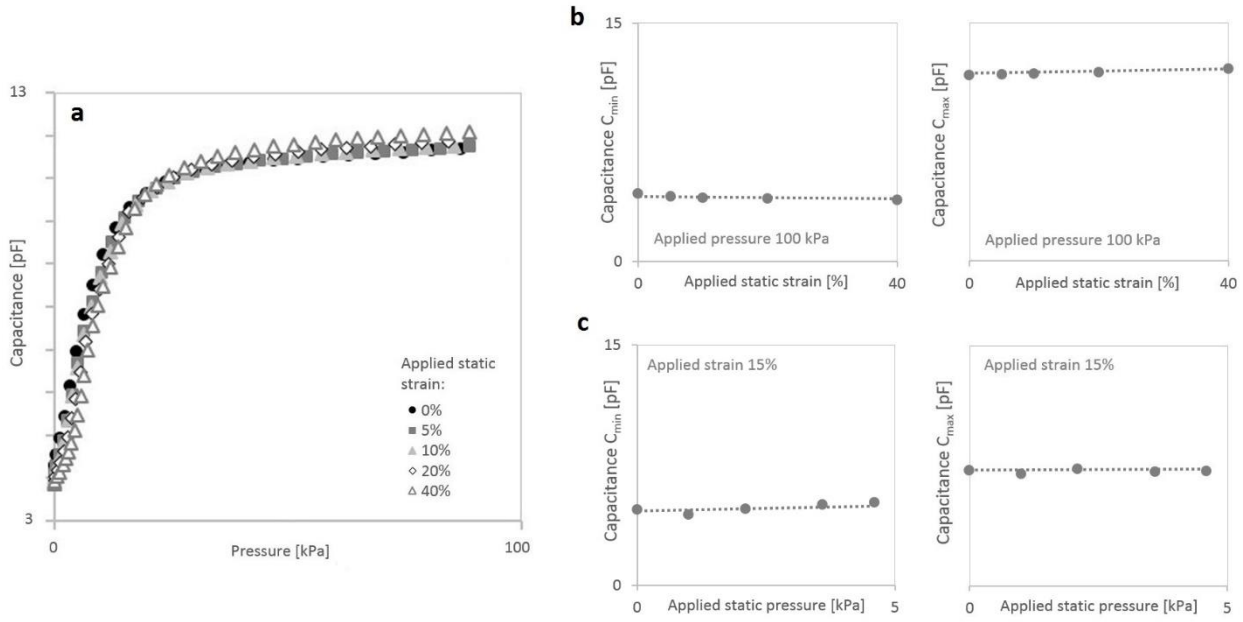

Supplementary Figure S3: a) Pressure sensor response. Measured capacitance as a function of applied pressure for applied static strains equal to 0%, 5%, 10%, 20% and 40%. b) Capacitances *Cmin* and *Cmax* measured at the minimum and maximal applied pressure, respectively, for applied static strains equal to 0%, 5%, 10%, 20% and 40%. c) Strain sensor response. Capacitances *Cmin* and *Cmax* measured at the minimum and maximal applied strain, respectively, for applied static pressures of 0 kPa, 1.0 kPa, 2.1 kPa, 3.6 kPa and 4.6 kPa.

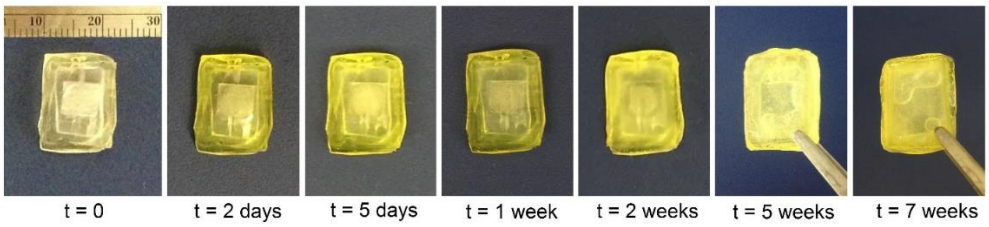

Supplementary Figure S4: *In vitro* degradation study of the strain and pressure sensor, showing that the device will degrade under biological conditions. The sensor was fully immersed in PBS solution at 37°C for 7 weeks. The sensor packaging, based on sealing with UV-exposed pre-POMaC, efficiently protects the metal electrodes from corrosion for the first 2 weeks. After this time, water infiltrates into the device, and a rapid corrosion of the electrodes occurs together with POMaC bulk erosion. The degradation process is slower *in vivo*, as illustrated in Fig. 4d and 4e where the sensors are still operational after 3.5 weeks of implantation *in vivo*.

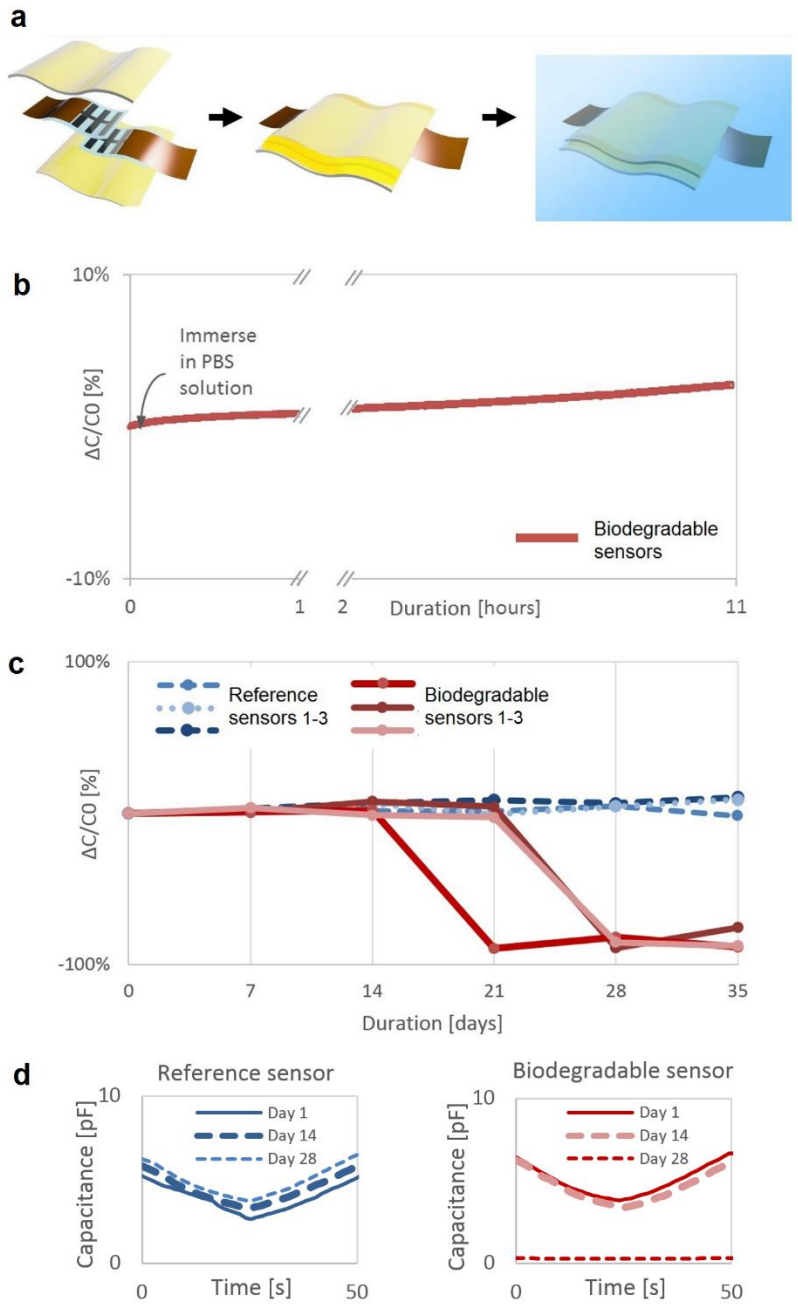

Supplementary Figure S5: Performance of the biodegradable sensor upon *in vitro* degradation. a) The *in vitro* study includes three biodegradable strain sensors (Mg electrodes evaporated on top of PLLA thin film and encapsulated into a POMaC packaging) and three reference non-biodegradable strain sensors (same design and dimensions as the biodegradable sensors except that the Mg electrodes are replaced by evaporated gold electrodes, and the packaging is made of PDMS – Polydimethylsiloxane – instead of POMaC). The sensors are fully immersed in phosphate buffered saline (PBS) solution at 25°C over 5 weeks. b) Capacitance of the biodegradable sensor measured in the first hours following the immersion in PBS solution, no strain applied. c) Capacitance measured on the three biodegradable strain sensors and three reference non-biodegradable strain sensors, no strain applied. After 3 weeks of incubation, the capacitances measured for the reference sensors is still within +/-10% of their initial value, while all the Mg electrodes of the biodegradable sensors are degraded. d) Response to applied strain measured after 1 day, 2 weeks and 4 weeks of immersion in PBS solution. The sensors are removed from PBS solution and dried in an oven at 40°C overnight. The biodegradable and reference sensors show similar responses excepted for the biodegradable sensor at day 28.